JOURNAL OF GEOPHYSICAL RESEARCH, VOL. 103, NO. D13, PAGES 16,369–16,383, JULY 20, 1998

Processes controlling the distribution of aerosol particles in the lower marine boundary layer during the First Aerosol Characterization Experiment (ACE 1)

Timothy S. Bates,[1,2,3] Vladimir N. Kapustin,[2,3] Patricia K. Quinn,[1,2] David S. Covert,[2,3] Derek J. Coffman,[2] Celine Mari,[4] Philip A. Durkee,[5] Warren J. De Bruyn,[6] and Eric S. Saltzman[6]

Abstract. The goals of the International Global Atmospheric Chemistry (IGAC) Program's First Aerosol Characterization Experiment (ACE 1) are to determine and understand the properties and controlling factors of the aerosol in the remote marine atmosphere that are relevant to radiative forcing and climate. A key question in terms of this goal and the overall biogeochemical sulfur cycle is what factors control the formation, growth, and evolution of particles in the marine boundary layer (MBL). To address this question, simultaneous measurements of dimethylsulfide (DMS), sulfur dioxide (SO_2), the aerosol chemical mass size distribution, and the aerosol number size distribution from 5 to 10,000 nm diameter were made on the National Oceanic and Atmospheric Administration (NOAA) ship *Discoverer*. From these data we conclude that the background MBL aerosol during ACE 1 often was composed of four distinct modes: an ultrafine (UF) mode (Dp = 5–20 nm), an Aitken mode (Dp = 20–80 nm), an accumulation mode (Dp = 80–300 nm), and a coarse mode (Dp > 300 nm). The presence of UF mode particles in the MBL could be explained by convective mixing between the free troposphere (FT) and the MBL associated with cloud pumping and subsidence following cold frontal passages. There was no evidence of major new particle production in the MBL. Oceanic emissions of DMS appeared to contribute to the growth of Aitken and accumulation mode particles. Coarse mode particles were comprised primarily of sea salt. Although these particles result from turbulence at the air-sea interface, the instantaneous wind speed accounted for only one third of the variance in the coarse mode number concentration in this region.

1. Introduction

Global aerosol size distributions of mass, number, and chemical composition are needed to calculate the direct and indirect radiative forcing due to aerosol particles. Given the short lifetimes of particles in the troposphere and their resulting spatial (vertical and horizontal) and temporal variability, it is not economically feasible to develop an observational network to map global aerosol distributions at the resolution needed for climate models. Accurate assessments of current radiative forcing due to aerosols must therefore rely on chemical transport models to generate the needed global aerosol distributions. Chemical transport models, developed and verified under present-day conditions, can then be used to generate global aerosol distributions using different emission scenarios and thus provide the needed input for prognostic analyses of future radiative forcing and climate response.

To generate accurate global aerosol distributions, chemical transport models must incorporate the physical and chemical processes that transform natural and anthropogenically derived emissions of aerosols and their precursors into the heterogeneously dispersed aerosol distributions that exist in the atmosphere. Although global chemical transport models [*Taylor and Penner,*

[1]Pacific Marine Environmental Laboratory (PMEL), NOAA, Seattle, Washington.

[2]Joint Institute for the Study of the Atmosphere and Ocean (JISAO), University of Washington, Seattle.

[3]Department of Atmospheric Sciences, University of Washington, Seattle.

[4]Laboratoire d'Aerologie, UMR, Université Paul Sabatier, CNRS, Toulouse, France.

[5]Department of Meteorology, Naval Postgraduate School, Monterey, California.

[6]Rosenstiel School of Marine and Atmospheric Science, University of Miami, Miami, Florida.

Paper number 97JD03720.
0148-0227/98/97JD-03720$09.00

1994; *Pham et al.*, 1995; *Chin et al.*, 1996; *Feichter et al.*, 1996; *Kasibhatla et al.*, 1997] and coupled climate chemistry models [*Chuang et al.*, 1997] continue to refine estimates of tropospheric aerosol distributions and the resulting radiative effects, reducing the uncertainties in these model estimates requires "more detailed and comprehensive data sets" [*Kasibhatla et al.*, 1997, p. 3757] of aerosol properties and processes. These data sets can be acquired with a long-term global observation network and short-term intensive campaigns.

The spatial variability in aerosol properties and the interactions between the various chemical components require aerosol characterization and process studies in a globally representative range of natural and anthropogenically perturbed environments. Natural emissions and the resulting background aerosol are essential components of both chemical transport models and radiative forcing calculations. The reasons for this are several fold. First, the emissions of natural aerosols and their gaseous precursors can contribute significantly to the total aerosol burden over large areas of the Earth [*Chin and Jacob*, 1996]. Second, gaseous emissions from human sources can interact with the existing background aerosol to modify the aerosol mass and number distribution [i.e., *Sievering et al.*, 1995; *Chuang et al.*, 1997]. Third, since the different aerosol components interact with each other, the total aerosol distribution and resulting radiative effect are not necessarily the sum of the individual background and anthropogenic components. Fourth, radiative forcing is defined as the total radiative effect due to aerosols minus the radiative effect due to background aerosols. Without a knowledge of the background aerosol properties, it is not possible to accurately quantify the direct and indirect forcing resulting from anthropogenically derived emissions.

The gas and aerosol measurements made aboard *Discoverer* during the First Aerosol Characterization Experiment (ACE 1) provide a means to characterize aerosol properties and assess the processes controlling the aerosol distribution in the lower marine boundary layer (MBL) south of Tasmania (Figure 1). In this minimally polluted marine environment the background atmospheric aerosol is composed largely of only two aerosol types, a sea-salt component and a non-sea-salt (nss) sulfate component. The primary source of both components is thought to be the sea surface with sea-salt particles being injected directly into the atmosphere and the nss sulfate component coming from the air-sea exchange of one primary gaseous precursor, dimethylsulfide (DMS). Less certain are the controlling processes that determine the aerosol size or spatial distribution at any given time. In this paper we focus on the processes controlling the physical and chemical aerosol distribution in the lower MBL. In a companion paper [*Quinn et al.*, this issue] we discuss the effects of these distributions on the aerosol optical properties. Complementary descriptive aerosol data analyses from Macquarie Island [*Brechtel et al.*, this issue; *Kreidenweis et al.*, this issue] and the free troposphere [*Clarke et al.*, this issue] are included in this special section.

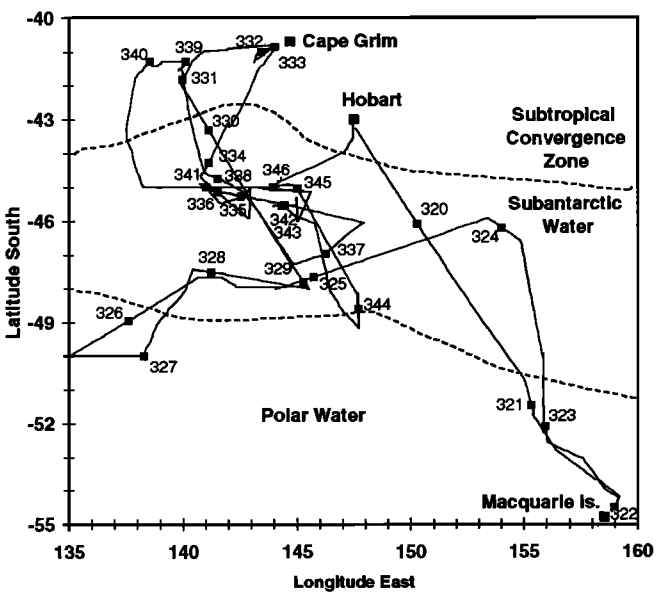

Figure 1. Discoverer cruise track during the intensive operations of ACE 1. The numbers (day of year in 1995) represent the ship's position at the beginning of each day (UTC). The three surface water masses are defined by salinity with subtropical convergence zone salinities >34.8 practical salinity unit (psu), Subantarctic water salinities >34.2 psu but <34.8 psu, and polar water salinities <34.2 psu.

2. Methods

Aerosol particles were sampled at 18 m above sea level through a heated mast [*Bates et al.*, this issue]. The mast extended 6 m above the aerosol measurement container and was capped with a rotating cone-shaped inlet nozzle that was positioned into the relative wind. Air was pulled through this 5-cm-diameter inlet nozzle at 1 m^3 min^{-1} and down the 20-cm-diameter mast. The lower 1.5 m of the mast were heated to dry the aerosol to a relative humidity (RH) of 40 to 50%. Fifteen 1.9-cm-diameter conductive tubes extending into this heated zone were used to isokinetically subsample the air stream for the various aerosol sizing instruments and impactors at flows of 30 L min^{-1}. Comparisons of the total particle count ($Dp > 5$ nm) during intercomparisons with the National Center for Atmospheric Research (NCAR) C-130 agreed to within 20%, suggesting minimal loss of particles in the inlet system.

The number size distribution between 5 and 600 nm was measured every 10 min with two differential mobility particle sizers (DMPS) at an RH of approximately 10%. The mobility distribution from the DMPSs was inverted to a number distribution by assuming that a Fuchs-Boltzman charge distribution resulted from the Kr^{85} charge neutralizer. The data were corrected for diffusional losses [*Covert et al.*, 1997] and size depen-

dent counting efficiencies [*Wiedensohler et al.*, 1997] based on the pre-ACE 1 intercalibration exercises. The number distribution between 0.6 and 9.6 μm was measured with an aerodynamic particle sizer (APS) at an RH of approximately 40%. Data at diameters larger than 5 μm were discarded due to interferences from phantom counts and uncertainties in large particle collection efficiencies. The APS diameters were converted to geometric diameters by dividing by the square root of the particle density and dried to 10% RH assuming a sea-salt growth factor of 1.5 between 40 and 10% RH [*Berg et al.*, this issue]. An interactive routine was used to fit lognormal curves to the different modes of the number size distribution.

Aerosol chemical sampling was conducted with Berner-type multijet cascade impactors. Air was sampled only when the relative wind direction was forward of the beam, the relative wind speed was greater than 3 m s^{-1}, and the total particle count indicated the air was free of ship contamination. Further details of the sampling and ion chromatographic and gravimetric analysis are reported elsewhere [*Quinn and Coffman*, this issue]. The 50% aerodynamic cutoff diameters of the impactors [*Quinn et al.*, this issue] were converted to geometric diameters by dividing by the square root of the particle density and dried to 10% RH assuming an ammonium bisulphate growth factor of 1.2 [*Berg et al.*, this issue].

Air samples for DMS analysis were collected through a Teflon line which ran approximately 60 m from the top of the aerosol sampling mast to the analytical system. One hundred mL min^{-1} of the 4 L min^{-1} flow were pulled through a KI solution at the analytical system to eliminate oxidant interferences [*Cooper and Saltzman*, 1993]. The air sample volume ranged from 0.5 to 1.5 L depending on the DMS concentration. Seawater samples were collected from the ship's seawater pumping system at a depth of approximately 5 m. The seawater line ran to the analytical system where 5.1 mL of sample were valved into a Teflon gas stripper. The samples were purged with hydrogen at 80 mL min^{-1} for 5 min. Water vapor in either the air or purged seawater sample stream was removed by passing the flow through a -25°C Teflon tube filled with silanized glass wool. DMS was then trapped in a -25°C Teflon tube filled with Tenax. During the sample trapping period, 6.2 pmol of methylethyl sulfide (MES) were valved into the hydrogen stream as an internal standard. At the end of the sampling/purge period the coolant was pushed away from the trap, and the trap was electrically heated. DMS was desorbed onto a DB-1 megabore fused silica column where the sulfur compounds were separated isothermally at 50°C and quantified with a sulfur chemiluminesence detector. The system was calibrated using gravimetrically calibrated DMS and MES permeation tubes. The precision of the analysis, based on both replicate analyses of a single water sample and replicate analyses of a standard introduced at the inlet of the air sample line, was typically ±8%. The detection limit during ACE 1 was approximately 0.8 pmol. The performance of the system was monitored regularly by running blanks and standards through the entire system. Values reported here have been corrected for recovery losses. Losses within the system were <10%. System blanks were below detection limit. Air samples are reported in units of nmol m^{-3} at standard temperature (25°C) and pressure (1013 mbar) such that 1 nmol m^{-3} equals 24.5 ppt.

Air was sampled for SO_2 analysis from the ship's flying bridge, 18 m above sea level [*Bates et al.*, this issue]. The inlet was heated and connected to a nafion dryer to minimize losses. The gaseous SO_2 in dry air was absorbed into an aqueous scrubbing solution in a gas/liquid exchange coil, converted to sulfite, and then derivatized to isoindole. The derivative was separated from interferents by isocratic reverse phase HPLC and detected by fluorescence. Further details of the instrument are reported elsewhere [*Saltzman et al.*, 1993; *De Bruyn et al.*, this issue]. The system was calibrated using a two-stage gas-dilution system with a low-level permeation device. The precision of replicate measurements was typically better than 5%, and the detection limit during ACE 1 was approximately 3–5 parts per trillion by volume (pptv). The performance of the system was monitored regularly by running blanks and standards through the entire system. Losses within the system were <15%. Values reported here have been corrected for recovery losses.

Additional measurements made aboard the ship included atmospheric temperature, pressure, and humidity, surface seawater temperature, salinity and nitrate concentrations, wind speed and direction, rainfall rates, solar radiation, atmospheric radon [*Whittlestone and Zahorowski*, this issue], and vertical profiles of temperature, dew point temperature, and wind speed and direction from radiosondes. All references to time are reported here in UTC which is 10 hours behind local standard time.

3. Results and Discussion

3.1. Characteristics of the MBL Aerosol

During the 29-day field experiment the ship encountered four episodes of continental air with high radon (>100 mBq m^{-3}) and total particle concentrations (2000–4000 cm^{-3}). These were generally on the back side of high-pressure systems which brought flow off the Australian continent. During the remainder of the month the air masses sampled at the ship were typical of background conditions in the midlatitudes [*Covert et al.*, 1996a] with very low radon concentrations (<100 mBq m^{-3}) and a mean total ($Dp > 5$ nm) particle number concentration of 500 cm^{-3} (Figure 2).

The particle number size distributions, $dN/d\log Dp$, fell into three distinct categories and could be modeled with generally three and sometimes four modes (Figure 3). All the distributions had a similar coarse mode (Dp = 300–5000 nm) comprised primarily of sea salt

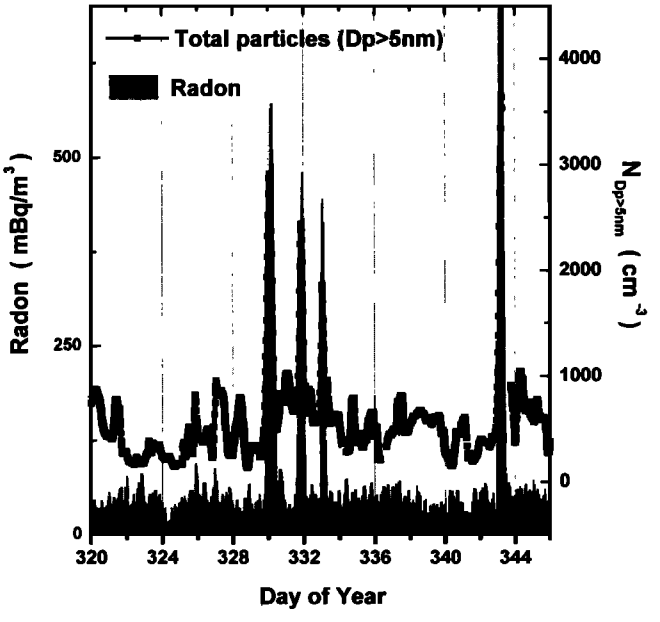

Figure 2. Total particle number concentration ($Dp >$ 5 nm) and atmospheric radon concentrations measured aboard *Discoverer* as a function of day of year (DOY).

(Table 1). The upper size on this mode was limited by instrumental uncertainties and sample inlet losses. The background marine distributions generally had distinct Aitken (Dp = 20–80 nm) and accumulation modes (Dp = 80–300 nm) with a minimum between the modes (60–100 nm). The aerosol mass in this size range ($Dp <$ 450 nm) was comprised primarily of nss sulfate, ammonium, methanesulfonate (MSA), and sea salt (Table 1). The sum of these ions ($Dp <$ 450 nm) were, on average, 100 ± 10% of the total gravimetric mass of particles with $Dp <$ 450 nm [*Quinn and Coffman*, this issue]. The average NH_4^+ to nss $SO_4^=$ molar ratio in this size range was 0.72 ± 0.23, suggesting only partly neutralized sulfuric acid particles. The presence of sea salt in this size range does not necessarily imply an additional sea-salt mode, but more likely represents the tail of the coarse mode extending into this size range [*Clarke and Porter*, 1993]. The presence of appreciable sea-salt mass in this size range has important implications for sea-salt aerosol lifetimes and the climatic effects of these particles [*Quinn et al.*, this issue].

The second most frequent size distribution (Figure 3) also occurred in background marine conditions, but had a fourth mode (Dp = 5–20 nm) which we refer to here as the ultrafine (UF) mode. This smallest mode is a short-lived transition from newly nucleated particles of a few nanometers diameter to the more stable Aitken mode centered around 30–40 nm [*Covert et al.*, 1996a, b; *Wiedensohler et al.*, 1996]. The UF mode was encountered at the ship 13 times, for periods ranging from 0.5 to 36 hours, during the 29-day experiment (Figure 4). The third type of size distribution occurred in continental air masses (Figure 3). There were once again three modes, although the number and mass concentrations in the Aitken and accumulation modes were much higher than in the background marine distributions and there was no clear concentration minimum between the modes.

3.2. Sources of Aerosol and Aerosol Precursors to the MBL

The ocean is a source of both sea-salt aerosol and nss sulfur to the MBL. The nss sulfur is emitted to the MBL primarily in the form of dimethylsulfide (DMS), a biologically produced trace gas [*Bates et al.*, 1994]. During ACE 1, seawater DMS concentrations (Table 2), which drive the ocean to atmosphere DMS flux, were highest in the subtropical convergence zone west of Tasmania (2.8 nM ± 1.2 nM). DMS concentrations in the subantarctic water (Figure 1) increased during the experiment. Initial concentrations (1.1 ± 0.3 nM) were very similar to the low concentrations observed in the polar water (0.9 ± 0.4 nM). During the latter part of the experiment, as the seasonal biological cycle progressed, Subantarctic water DMS concentrations (2.4 ± 1.0 nM) increased to levels similar to the subtropical convergence zone.

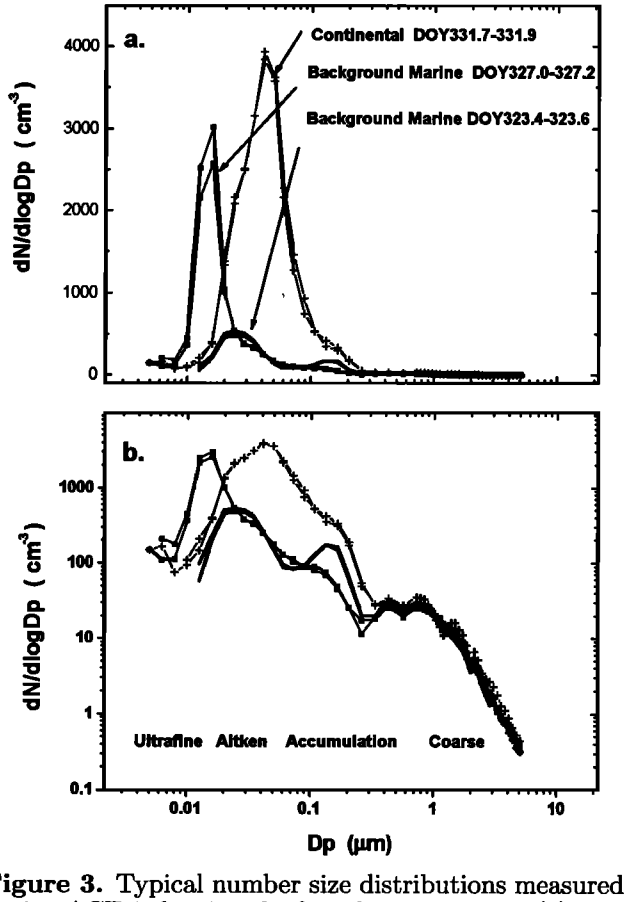

Figure 3. Typical number size distributions measured during ACE 1 showing the four distinct modes. (a) Linear and (b) logarithmic concentration plots are shown to present the entire range of data in perspective.

Table 1. Aerosol Number and Chemical Mass Characteristics Measured Aboard the NOAA Ship *Discoverer* During the ACE 1 Intensive (November 15 to December 14, 1995)

	Modes			
	Ultrafine	Aitken	Accumulation	Coarse
	Background Marine			
N, cm^{-3}	190	210	74	15
D_{gn}, nm	16	33	110	540
σ_g	1.45	1.40	1.41	2.02
Sea salt, ng m^{-3}			280	9,000
Range, ng m^{-3}			130–610	3,000–20,000
nss $SO_4^=$ + NH_4^+, ng m^{-3}			170	44
Range, ng m^{-3}			93–320	0–130
MSA, ng m^{-3}			31	23
Range, ng m^{-3}			10–180	5–67
	Continental			
N, cm^{-3}	500	720	75	23
D_{gn}, nm	18	37	130	530
σ_g	1.42	1.50	1.32	2.08

The mean number concentration, number mean geometric diameter at 10% RH, and standard deviation of the averaged data were determined from a log normal fit to the modes. The chemical concentrations are given as <450 nm geometric diameter at 10% RH (first three impactor stages [*Quinn et al.*, this issue] and >450 nm mass concentrations.

The flux of DMS to the atmosphere is calculated from the seawater DMS concentration and wind speed. Two wind speed transfer velocity relationships [*Liss and Merlivat*, 1986; *Wanninkhof*, 1992] currently used to calculate air-sea gas exchange result in fluxes that vary by roughly a factor of 2 (Table 2). Using these two relationships to estimate the range of DMS fluxes in the ACE 1 region results in calculated median DMS fluxes of 2.3 to 4.1 μmol m^{-2} d^{-1} in the polar waters, 3.0 to 7.3 μmol m^{-2} d^{-1} in the Subantarctic water, and 5.4 to 8.9 μmol m^{-2} d^{-1} in the subtropical convergence zone (Table 2). The ocean-atmosphere flux of DMS in the

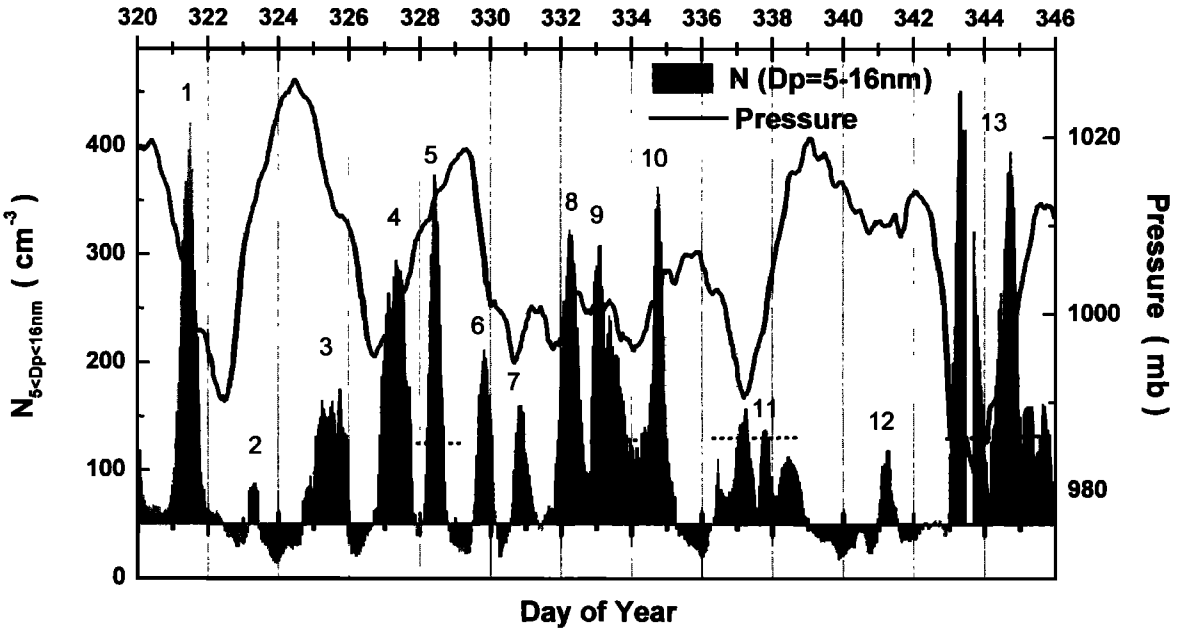

Figure 4. Total number concentration of particles with diameters between 5 and 16 nm plotted with atmospheric pressure as a function of DOY. A particle threshold of 50 cm^{-3} is used to more clearly delineate the 13 UF particle events.

Table 2. Measured Seawater and Atmospheric DMS Concentrations Associated With the Three Surface Water Masses in the ACE 1 Study Area (Figure 1)

	Seawater DMS, nM	Atmospheric DMS, nmol m^{-3}	DMS Flux [*Liss and Merlivat*, 1986], μmol m^{-2} d^{-1}	DMS Flux [*Wanninkhof*, 1992], μmol m^{-2} d^{-1}
Polar water				
Median	0.79	3.3	2.3	4.1
Average	0.90	4.1	3.4	6.1
Standard deviation (1σ)	0.39	2.3	2.7	5.2
Range	0.5–2.9	1.7–9.7	0–11	0.3–21
Subantarctic water (DOY 320–338)				
Median	1.09	3.0	3.0	5.2
Average	1.10	3.3	3.0	5.6
Standard Deviation (1σ)	0.31	1.4	2.0	3.9
Range	0.4–2.4	1.0–9.2	0–9.7	0–19
Subantarctic water (DOY 338–346)				
Median	2.24	5.6	4.5	7.3
Average	2.43	6.0	6.6	11.6
Standard Deviation (1σ)	1.00	2.9	7.3	13.7
Range	0.9–5.6	1.0–14.2	0–46	0–85
Subtropical Convergence Zone				
Median	2.60	4.9	5.4	8.9
Average	2.84	5.5	6.9	12.6
Standard Deviation (1σ)	1.21	2.6	5.7	10.8
Range	0.8–6.8	1.7–14.3	0–33	0–61

DMS fluxes were calculated for each seawater measurement, using the in-situ wind speed and the wind speed transfer velocity relationships of both *Liss and Merlivat* [1986] and *Wanninkhof* [1992].

polar waters is typical of winter fluxes at this latitude, while the fluxes calculated for the Subantarctic waters late in the experiment and the subtropical convergence zone waters during the entire ACE 1 were more typical of summer conditions [*Bates et al.*, 1987].

The ocean-atmosphere flux of DMS during ACE 1 maintained an atmospheric DMS concentration of 1 to 14 nmol m^{-3} (Table 2) with an overall mean concentration of 4.5 $\pm$ 2.5 nmol m^{-3}. This concentration is nearly identical to the mean December DMS concentration (4.9 nmol m^{-3}) measured at Cape Grim from 1988 to 1992 [*Ayers et al.*, 1995]. DMS in the MBL has two major sinks, transport to the free troposphere (FT) and oxidation in the MBL by OH [*Ayers et al.*, 1995; *Bandy et al.*, 1996; *Yvon et al.*, 1996]. The oxidation of DMS by OH proceeds by two pathways and can yield a variety of gas phase products including dimethylsulfoxide, dimethylsulfone, SO_2, MSA, and sulfuric acid [*Berresheim et al.*, 1995]. SO_2, the only gas phase DMS oxidation product measured aboard *Discoverer*, was present at an average concentration of 0.5 $\pm$ 0.3 nmol m^{-3}. Some fraction of the gas phase DMS oxidation products will nucleate new particles or condense/react onto existing particles in the MBL depending primarily on the existing particle surface area [*Covert et al.*, 1996a].

The ocean is a source of sea-salt particles to the atmosphere through the bursting of air bubbles associated with breaking waves (film and jet droplets) and the mechanical tearing (spume droplets) and spilling over (splash droplets) of wave crests (reviewed by *Andreas et al.* [1995]). While the total number concentration of these mechanically produced sea-salt particles is relatively small even in the remote MBL (Figure 2 and Table 1), they can dominate the mass size distribution (Table 1 and *Quinn et al.* [1996]) and thus have a significant effect on chemical reactions occurring in the MBL [*Sievering et al.*, 1992], the formation of new particles [*Covert et al.*, 1996a, b], the production of cloud condensation nuclei [*O'Dowd et al.*, 1997], and the light scattering by aerosols [*Quinn et al.*, 1996; this issue]. The magnitude of the ocean-atmosphere flux of sea-salt particles is a function of the wind-dependent sea state [*Monahan et al.*, 1986], while the instantaneous atmospheric sea-salt distribution is a function of the ocean-atmosphere flux, mixing between the MBL and FT, size-dependent removal processes, and advection.

The FT also can be a source of aerosol and aerosol precursors to the MBL. Long-range transport of SO_2 from the continents can bring anthropogenically and volcanically derived SO_2 to remote regions where it can be entrained into the MBL [*Andreae et al.*, 1988; *Thornton et al.*, 1996]. This did not appear to be the case during ACE 1 as SO_2 concentrations generally decreased with altitude above the MBL (A. Bandy, personal communication, 1997). The low concentrations of SO_2 in the FT and the presence of DMS in the FT (A. Bandy, personal communication, 1997) suggest a MBL source for the FT sulfur in this region.

Aerosol concentrations in the remote FT can also be

high due to long-range transport of continental aerosols [*Clarke et al.*, 1996] and the in situ production of UF particles [*Hegg et al.*, 1990; *Clarke*, 1993; *Perry and Hobbs*, 1994]. Aerosol distributions, soot concentrations, and volatility measurements in the FT during ACE 1 [*Clarke et al.*, this issue] indicate a low concentration of continental aerosol. The FT therefore appears to be a minimal source of aerosol mass to the MBL. However, high concentrations of newly formed UF particles were often observed in the FT in the vicinity of both low and high level clouds [*Clarke et al.*, this issue]. The large number concentrations of these UF particles could have a major impact on the MBL particle concentrations during periods of strong subsidence and entrainment from the FT. Modeling studies [*Raes and Van Dingenen*, 1992; *Raes*, 1995] and previous observations [*Clarke*, 1993; *Covert et al.*, 1996a, b; *Bigg et al.*, 1996] have shown that this process can be a ma-

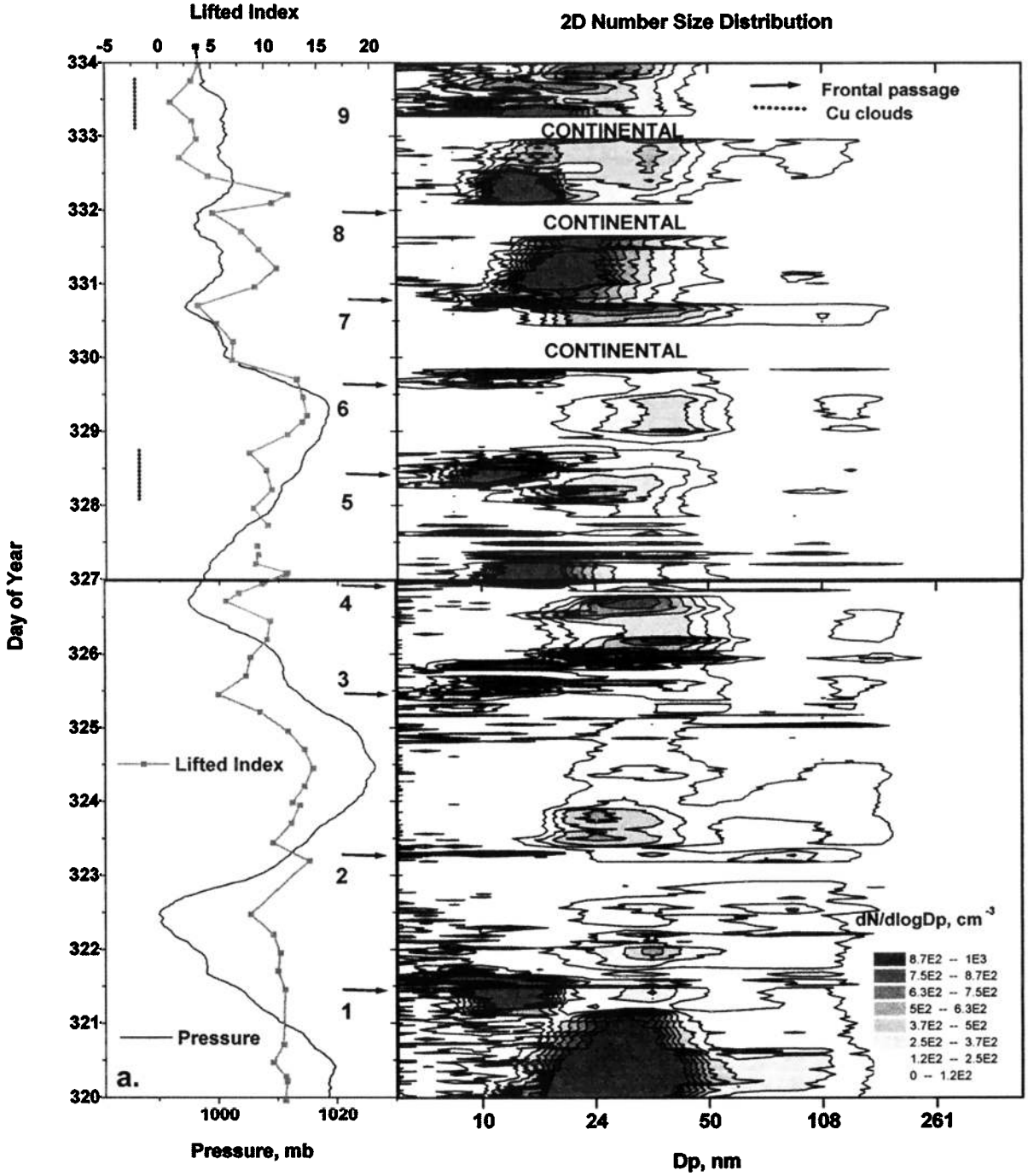

Figure 5. Contour plots of the number size distributions measured during ACE 1 during background marine conditions. The 13 UF particle events shown in Figure 4 are labeled. Each event can be attributed to either the passage of a cold front (arrow) or a cumulus cloud field (dots). Also plotted are atmospheric pressure and the lifted index (LI) which was generated from the shipboard radiosonde data. (a) DOY 320–334, (b) DOY 334–347.

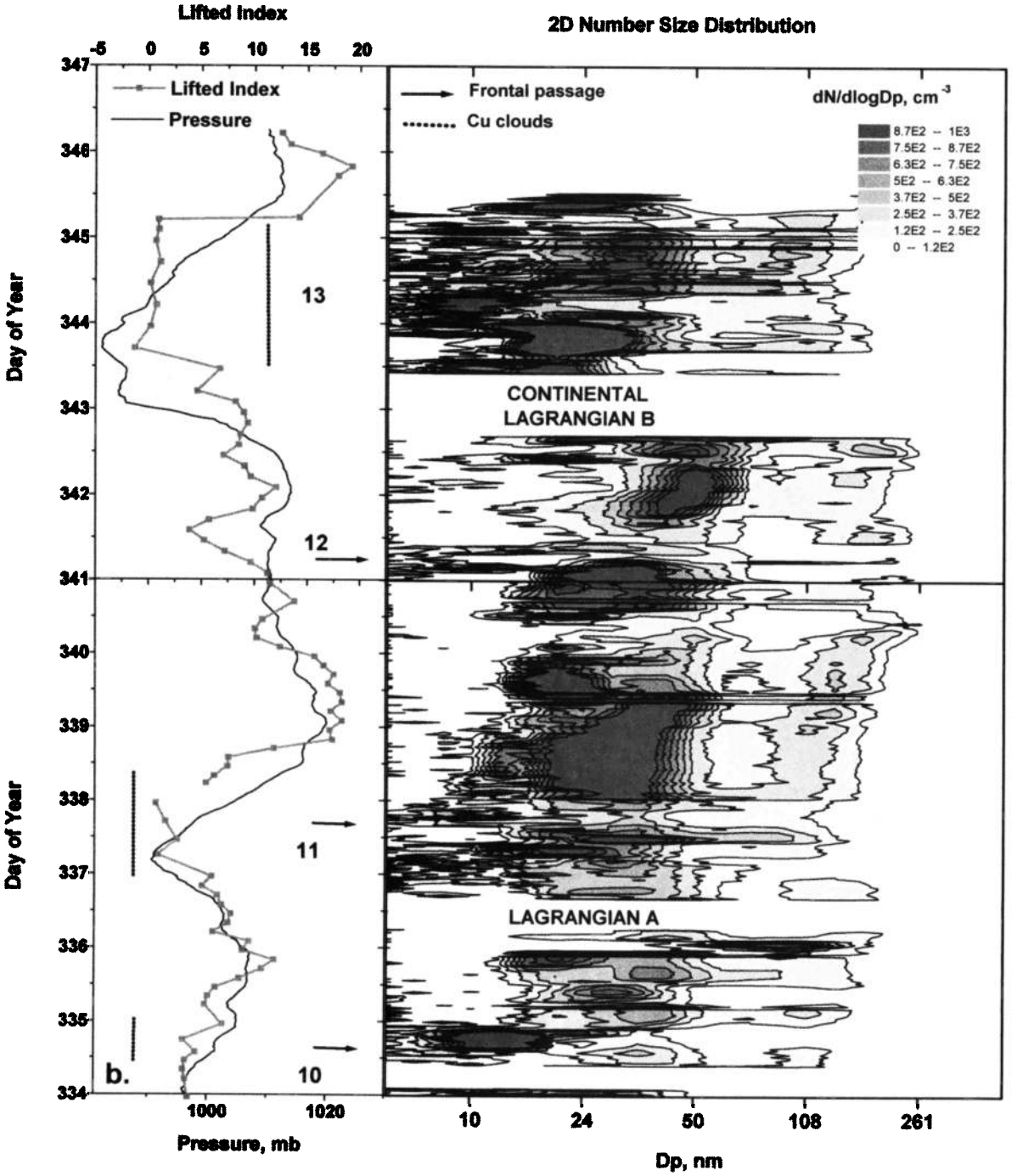

Figure 5. (continued)

jor source of new submicrometer aerosol to the remote MBL.

3.3. Processes Controlling the MBL Aerosol

High concentrations (>50 particles cm^{-3}) of UF mode particles (Dp = 5–20 nm) were observed aboard *Discoverer* approximately 50% of the time during ACE 1, occurring as 13 separate events (Figures 4 and 5). Measurements during ACE 1 [*Clarke et al.*, this issue; *Weber et al.*, this issue], previous studies [*Shaw*, 1989; *Covert et al.*, 1992; *Weber et al.*, 1995, 1996, 1997], and model calculations [*Hegg et al.*, 1992; *Russell et al.*, 1994; *Raes*, 1995] have shown that UF mode particle production is critically dependent upon H_2SO_4 concentrations and preexisting aerosol surface area concentrations. Model calculations using typical MBL conditions suggest that preexisting surface areas must be less than 5 μm^2 cm^{-3} [*Hegg et al.*, 1992] or 25 μm^2 cm^{-3} [*Raes*, 1995] for in situ particle formation to occur. During ACE 1 there was no correlation between the concentration of the H_2SO_4 precursors (DMS and SO_2) measured aboard *Discoverer* and the observed UF mode particle concentrations. Furthermore, the average preexisting aerosol surface area measured 18 m above the sea surface dur-

ing the 13 UF events ranged from 40 to 130 μm^2 cm^{-3} at ambient RH. This surface area concentration would likely suppress new particle production and high UF mode particle concentrations by scavenging condensable vapors, clusters, and newly formed particles [*Shaw*, 1989; *Covert et al.*, 1992; *Raes*, 1995; *Weber et al.*, 1995].

Conditions in the FT and the cloud-topped boundary between the MBL and FT are often more favorable for new particle production than the conditions which generally exist in the MBL [*Hegg et al.*, 1990; *Raes and Van Dingenen*, 1992; *Clarke*, 1993; *Hoppel et al.*, 1994a; *Raes*, 1995; *Covert et al.*, 1996a, b]. The UF particles produced aloft can be entrained into the MBL. During ACE 1, most of the observed UF events (1–8 and 10–12, Figures 4 and 5) coincided with the passage of cold fronts and the postfrontal subsidence associated with them [*Bond and Fleagle*, 1988]. For example (Figure 6), the prefrontal air mass sampled at the ship at the end of day 331 had passed over the Australian continent picking up radon. The passage of the front, which began with a brief rain event, was marked by a change in wind

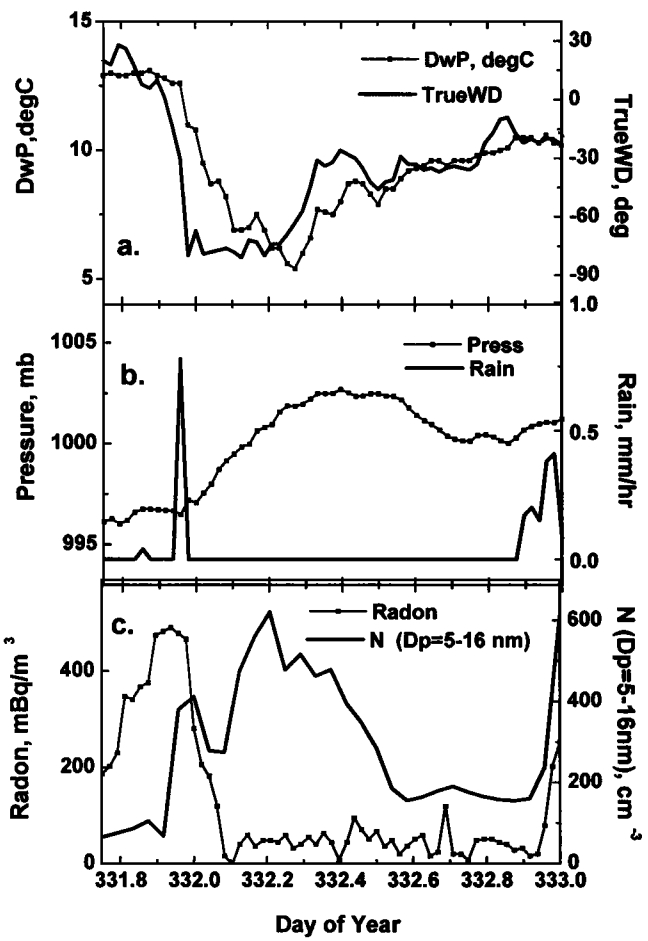

Figure 6. Aerosol and meteorological data for a frontal passage on DOY 332. (a) True wind direction and dew point temperature, (b) atmospheric pressure and rainfall rate, (c) radon concentrations and number of particles with diameters between 5 and 16 nm.

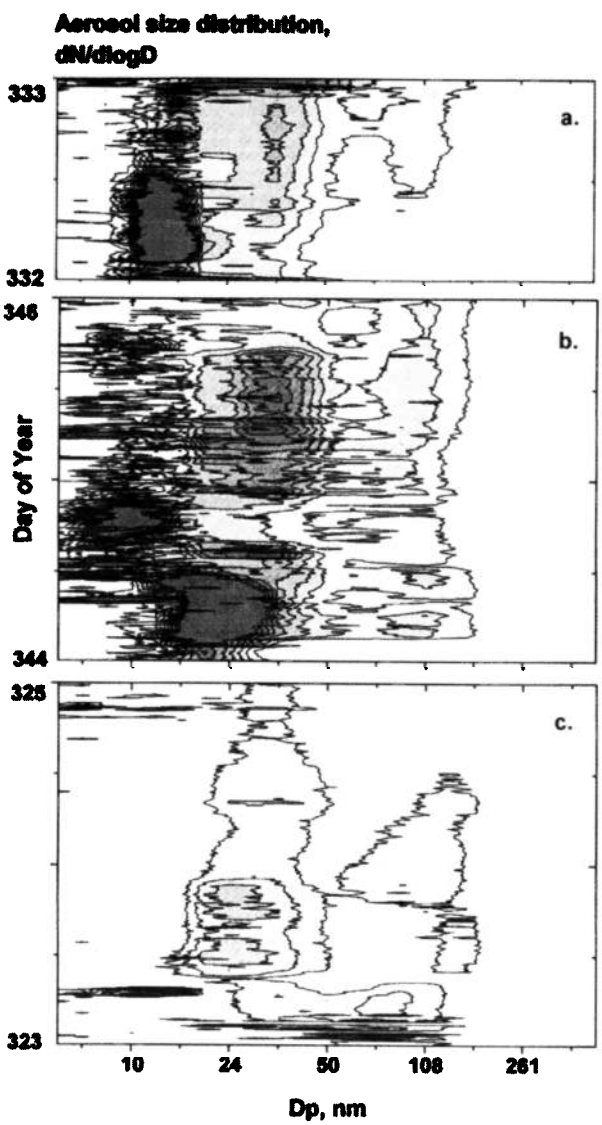

Figure 7. Contour plots of the number size distribution for (a) the frontal passage on DOY 332, (b) the cumulus cloud mixing period during DOY 344–346, and (c) the stratus cloud period during DOY 323–325. The scale is the same as in Figure 5.

direction and depression in dew point temperature. The air mass behind the front had not been in recent contact with the continent based on low radon values. The aerosol surface area during this period (day of year (DOY) 331–333) was always >84 μm^2 cm^{-3}, and thus was not conducive to new particle production [*Clarke et al.*, this issue]. However, UF particles with diameters between 10 and 20 nm appeared in this air mass after the frontal passage (Figures 6 and 7a). During DOY 332, measurements aboard the NCAR-130 revealed layers of high concentrations (2000 to 4000 cm^{-3}) of small UF particles (narrow mode centered at about 12 nm) in the broken convective cloud region behind the front [*Clarke et al.*, this issue]. The layers occurred between 2 and 4 km and were associated with cloud outflows. In

the cloud-free region of postfrontal subsidence, elevated concentrations of UF particles in the 10 to 20 nm size range extended down to the MBL inversion [*Clarke et al.*, this issue]. On the basis of these data the most likely source of the UF particles measured aboard *Discoverer* in the lower MBL was entrainment from aloft. Although not all the frontal passages and UF events are as clear as this example, many show similar features that support the hypothesis that UF particles are produced in the FT or upper MBL and mixed down into the lower MBL.

Other UF events (5, 9, 10, 11, and 13, Figure 5), often with higher concentrations of particles <10 nm diameter and more variable concentrations of UF mode particles (Figure 7b), appeared to coincide with regions of active cumulus clouds [*Cotton et al.*, 1995]. The degree of convective activity was estimated from the lifted index (LI) which was calculated from the shipboard radiosonde data [*Galway*, 1956]. Mathematically, LI = $T_{500} - T_L$, where T_{500} is the in-situ temperature at 500 mbar and T_L is the resultant temperature after a moist adiabatic lifting of an air parcel within the MBL to 500 mbar. Lower values of LI, indicating greater instability, coincided with UF events 9, 10, 11, and 13 (Figure 5). Event 13, for example, occurred in a field of broken cumulus clouds. The temperature/dew point sounding from *Discoverer* on DOY 344 (Figure 8b) showed a capping inversion at 350 mbar and a relatively deep boundary layer extending to 700 mbar (–20°C). Advanced very high resolution radiometer (AVHRR) satellite data showed that cloud tops frequently extended above the boundary layer (cloud top temperatures <–20°C). These active cumulus clouds vent gases from the MBL to the free troposphere where conditions favor the formation of new particles [*Perry and Hobbs*, 1994; *Raes*, 1995; *Clarke et al.*, this issue]. The photochemical production of new particles in the cloud processes air was observed in this region on DOY 334 [*Clarke et al.*, this issue]. To balance the cumulus updrafts, air can descend in the cloud-free air between clouds [*Cotton et al.*, 1995], providing a transport mechanism to bring UF particles to the MBL. A contrasting case occurred on DOY 323 where stratus clouds with cloud-top temperatures of –5°C capped the well-defined boundary layer at 850 mbar (Figure 8a). Here there was little exchange with the FT and no evidence of UF particles (Figure 7c).

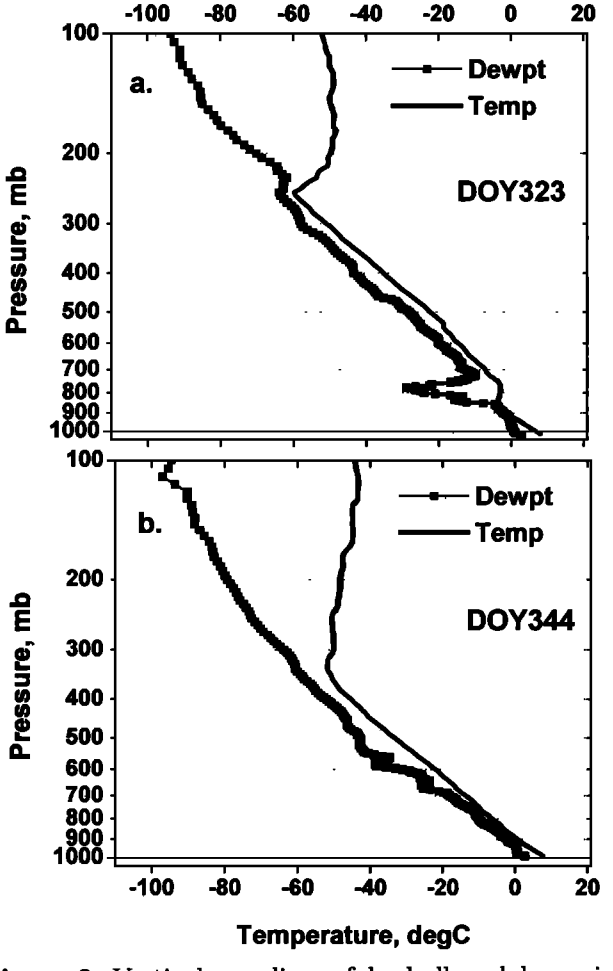

Figure 8. Vertical soundings of dry bulb and dew point temperatures from radiosondes launched from *Discoverer* on (a) DOY 323 at 1700 where *Discoverer* was located under a stratus cloud deck and (b) DOY 344 at 1100 where *Discoverer* was located in a region of cumulus clouds.

MBL Aitken mode particles originate from the condensational growth and coagulation of UF mode particles [*Hoppel et al.*, 1990; *Weber and McMurry*, 1996] and from entrainment from aloft [*Clarke et al.*, 1996]. As Aitken mode particles are mixed within the MBL, they are "processed" by clouds and grow by liquid phase conversion of trace gases to nonvolatile solute compounds and by coagulation with other Aitken and UF mode particles [*Hoppel and Frick*, 1990]. On the basis of the water supersaturation level in the cloud, some particles will eventually grow sufficiently large to activate and form cloud droplets. When the cloud dissipates, the interstitial (unactivated) particles and residual (from evaporated cloud droplets) particles remain. This process is thought to differentiate the Aitken and accumulation modes with the MBL cloud supersaturation and aerosol chemistry defining the diameter of the intermode minimum [*Hoppel et al.*, 1986, 1994a, b]. On average, particles will be cycled through many nonprecipitating clouds before being removed by rain [*Hoppel and Frick*, 1990]. Thus cloud processing will occur multiple times to create and magnify this bimodal feature.

Clouds were a dominant meteorological feature in the ACE 1 study area. Frontal passages and subsidence around venting clouds introduced Aitken mode particles and their UF mode precursors to the MBL. However, it is not possible to directly attribute any increase in Aitken mode number to the frequent high concentrations of UF mode particles (Figure 4) since the shipboard observations are not Lagrangian. The frequent

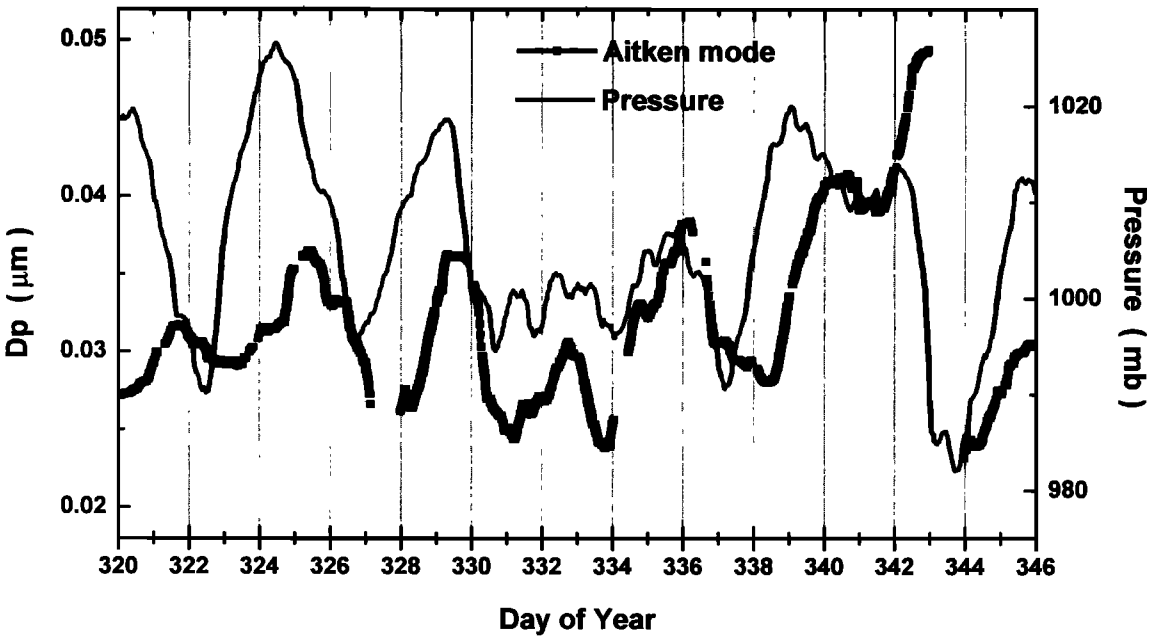

Figure 9. Twenty-four hour geometric, number mean diameter, D_{gn}, of the Aitken mode and atmospheric pressure as a function of DOY.

abrupt changes in the aerosol size distribution (Figure 5) are also evidence that the system was rarely in steady state. Still, there are several re-occurring features in the data. In general, the diameter of the Aitken mode increased with time in high-pressure systems (Figure 9), which is consistent with increased condensational growth in the MBL and reduced vertical entrainment through a well-capped boundary layer. Calculated isokinetic back trajectories suggest that the air mass stayed in the MBL (RH 60–70%) for several days. In contrast, the Aitken mode diameter either decreased or was low during periods of frontal passages and convective subsidence, presumably due to mixing of smaller, less aged particles from the FT. Elevated concentrations of UF particles and lower concentrations of Aitken mode particles existed just above the MBL in these regions [*Clarke et al.*, this issue].

The period from DOY 337 to DOY 341 is shown in more detail in Figure 10. The frontal passage with associated rainfall occurred at the beginning of DOY 337 (Figure 10a). The trough following the front generated a large area of cumuliform clouds which brought UF particles to the MBL through DOY 338 (Figure 4). The photochemically generated SO_2 [*De Bruyn et al.*, this issue] provided a source of sulfur for both condensational particle growth and within-cloud liquid phase growth (Figure 10b). During this period the average Aitken and accumulation mode diameters remained constant (Figure 10c), presumably due to a balance between the effects of mixing from the FT and growth within the MBL. As the high-pressure system passed, a field of broken stratocumulus clouds capped the boundary layer at 880 mbar. During DOY 339 and 340 the Aitken mode diameter appeared to grow during the day, while the mean diameter of the accumulation mode constantly increased. A rain event (Figure 10a) may have been responsible for the decrease in mean modal diameters at DOY 340.5. Again, these observations did not follow a specific air mass, and thus the observed changes could be simply due to advection. Still, the data are consistent with the cloud processing described above.

A key question in this study is whether the emissions of DMS from the ocean can quantitatively account for the nss sulfate in marine aerosols. The frequent frontal passages and mixing between the MBL and FT complicate a regionally averaged assessment of this question. Given the average atmospheric DMS concentration (Table 2), an average 1 km well-mixed boundary layer, and the calculated ocean-atmosphere DMS fluxes (Table 2), the lifetime of DMS in the MBL in this region is approximately 1 day. Photochemical model calculations indicate that 30–50% of this DMS is converted to SO_2 [*De Bruyn et al.*, this issue]. The diurnal cycles of SO_2 during DOY 337 to DOY 341 (Figure 10b) are evidence of a daytime photolytic production coupled with a continuous loss to aerosol and surface dry deposition. Using a regional average OH concentration of 6×10^{-5} mol cm^{-3} [*Spivakovsky et al.*, 1990] and an OH + SO_2 reaction rate constant of 9.5×10^{-13} [*DeMore et al.*, 1992], we can estimate the mean photochemical production rate of H_2SO_4 from observed SO_2 concentrations. The average photochemical production rate of H_2SO_4 for the period DOY 339 to DOY 341 is 260 mol cm^{-3} s^{-1}. Using the observed aerosol surface areas, we can then estimate the average steady state H_2SO_4 concentration and the flux of H_2SO_4 to each aerosol mode.

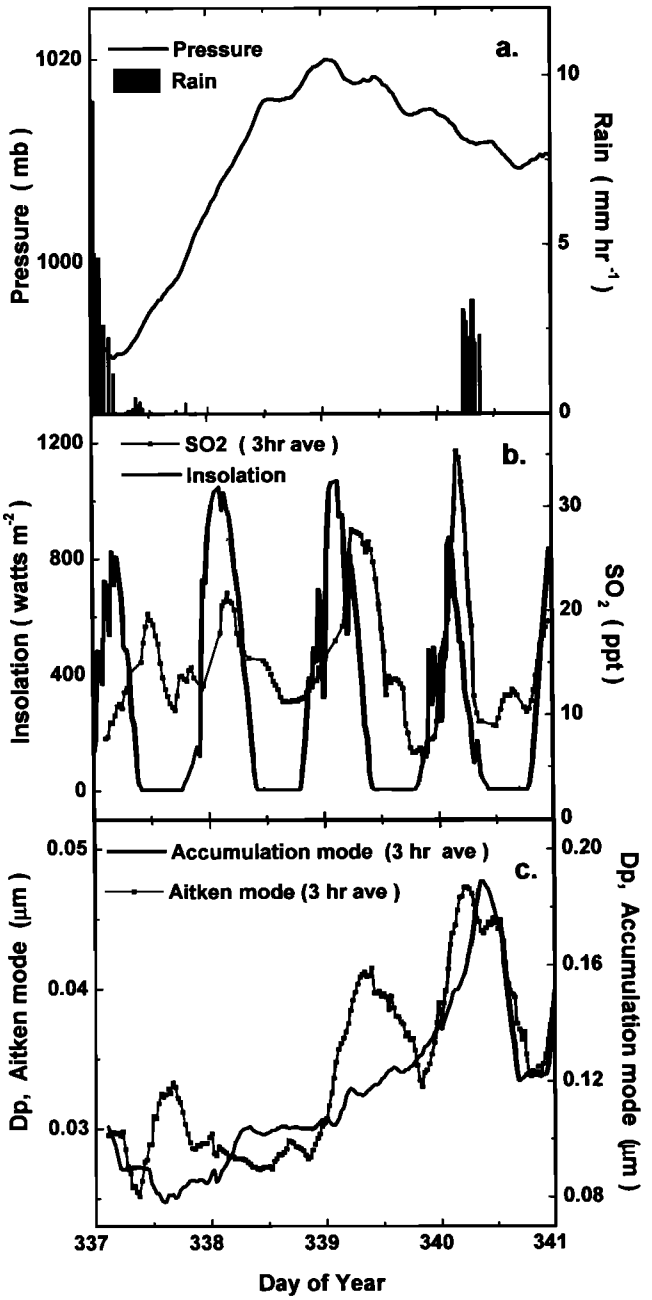

Figure 10. (a) Atmospheric pressure (millibars) and rainfall rate (mm hr^{-1}), (b) solar insolation (W m^{-2}) and 3-hour average SO_2 concentrations (ppt), and (c) 3-hour average diameters of the Aitken and accumulation modes (micrometers) as a function of DOY.

The average steady state H_2SO_4 concentration for the period DOY 337 to DOY 341 is 0.014 pptv. The flux of H_2SO_4 to accumulation mode aerosols is estimated to be 1.7×10^{-17} mol S cm^{-3} d^{-1}. The observed increase in the accumulation mode diameter (Figure 10c) for the 100 particles cm^{-3} present corresponds to a mass increase of 2×10^{-17} mol S cm^{-3} d^{-1}. While again, these observations did not follow a specific air mass and thus the observed changes could be due to advection, the ocean-atmosphere flux of DMS, its conversion to SO_2, its oxidation to H_2SO_4, and the subsequent flux of H_2SO_4 to existing particles is sufficient to explain the observed growth in this mode.

The coarse mode, which consisted almost entirely of sea salt (Table 1), had an average number concentration 18 m above the sea surface of 15 ± 9.6 particles cm^{-3} (Figure 11a). The number mean diameter of this mode was relatively constant at 540 ± 73 nm (at 10% RH). Particles in this size range have a residence time of approximately 2 days [*Gong et al.*, 1997], and thus the number concentration is determined by the balance of source and sink processes integrated over this time period. Sea-salt aerosols in this size range have been shown to have a strong exponential dependence on wind speed [*O'Dowd and Smith*, 1993]. A similar analysis of the ACE 1 coarse mode data shows that the instantaneous wind speed can account for approximately one third ($R^2 = 0.32$) of the variance (Figure 11b). This low correlation is not surprising given the highly variable wind speed over the region and regular frontal passages during the month-long study [*Hainsworth et al.*, this issue] in comparison to the 2-day residence time of the aerosol. Wind speeds measured at the ship varied from 0 to 22 m s^{-1} with a mean of 9.5 ± 3.8 m s^{-1} (Figure 11a). However, the winds, measured at the ship, do not necessarily reflect the wind/wave history experienced by the air parcel in the 2-day period prior to arriving at the ship. Sink processes, that is, wet and dry deposition and vertical turbulent transport, also vary with wind speed and frontal passages. The time and space variability in the processes controlling the sea-salt number concentrations require the use of regional aerosol transport models driven by observation-derived meteorology to better describe the fluctuations in the sea-salt number concentration. Local instantaneous wind speed is not a good indicator of sea-salt number concentrations in regions of rapidly varying wind speeds.

4. Conclusions

The MBL aerosol in the region south of Australia was composed of four distinct modes with a mean total particle number concentration of 500 cm^{-3}. The dominant process affecting the three smaller modes was the dynamical mixing between the FT and MBL which brought UF mode particles from the FT to the MBL and diluted the Aitken and accumulation mode populations. During the 29-day experiment an UF mode was observed approximately 50% of the time and coincided with the passage of cold fronts, postfrontal subsidence, or cloud pumping. There was no evidence of major new particle production in the MBL. The mean diameters of Aitken and accumulation mode particles increased in air masses that had been in the MBL for longer periods of time suggesting growth from the DMS sulfur that was emitted from the ocean to the MBL. Photochemical model calculations showed that the emissions of DMS could quantitatively account for the observed particle

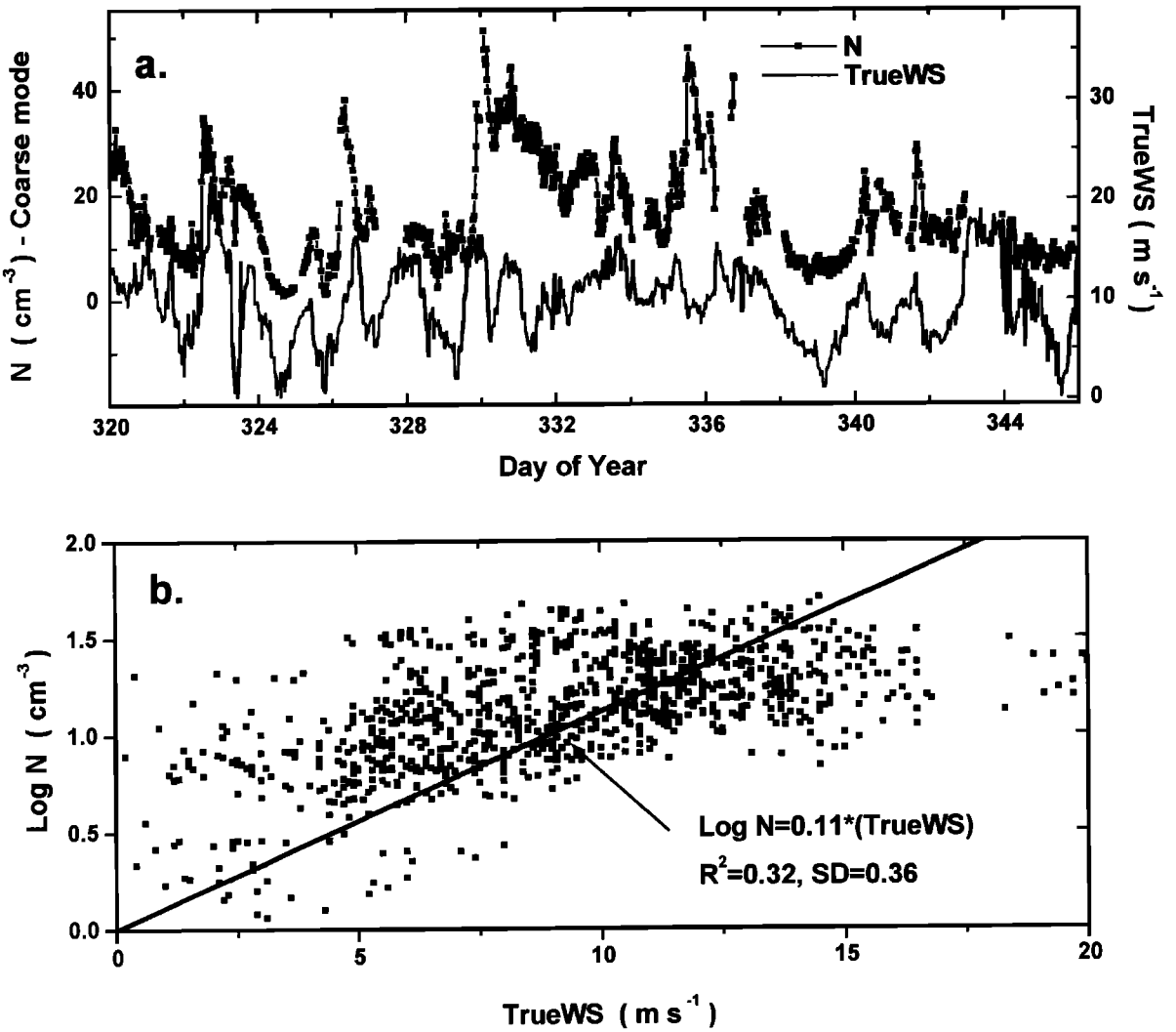

Figure 11. Total number concentration in the coarse mode (particles per cubic centimeters) and true wind speed (WS) (in m s^{-1}) measured aboard *Discoverer* plotted (a) as a function of day of year and (b) as a logarithmic regression of half-hourly data.

growth. The coarse mode was dominated by sea salt. However, in this region of rapidly changing wind speed, the local instantaneous wind speed accounted for only one third of the variance in the number concentration of the coarse mode.

Acknowledgments. We thank J. Johnson, D. Hamilton, M. Hamilton, S. Whittlestone, K. Nielsen, C. Skupniewicz, and K. Knudson for their assistance, the officers and crew of the NOAA ship *Discoverer* for their cooperation and support, the NCAR Atmospheric Technology Division (ATD) for the atmospheric sounding data, and A. Clarke, K. Suhre, E. Swietlicki, and R. Weber for their reviews of this manuscript. This research was funded by the Aerosol Project of the NOAA Climate and Global Change Program. This research is a contribution to the International Global Atmospheric Chemistry (IGAC) Core Project of the International Geosphere-Biosphere Programme (IGBP) and is part of the IGAC Aerosol Characterization Experiments (ACE). This is NOAA/PMEL contribution 1854 and JISAO contribution 441.

References

Andreae, M. O., H. Berresheim, T. W. Andreae, M. A. Kritz, T. S. Bates, and J. T. Merrill, Vertical distribution of dimethylsulfide, sulfur dioxide, formic acid, aerosol ions, and radon over the northeast Pacific Ocean, *J. Atmos. Chem.*, *6*, 149–173, 1988.

Andreas, E. L., J. B. Edson, E. C. Monahan, M. P. Rouault, and S. D. Smith, The spray contribution to net evaporation from the sea: A review of recent progress, *Boundary Layer Meteorol.*, *72*, 3–52, 1995.

Ayers, G. P., S. T. Bentley, J. P. Ivey, and B. W. Forgan, Dimethylsulfide in marine air at Cape Grim, 41°S, *J. Geophys. Res.*, *100*, 21,013–21,021, 1995.

Bandy, A. R., D. C. Thornton, B. W. Blomquist, S. Chen, T. P. Wade, J. C. Ianni, G. M. Mitchell, and W. Nadler, Chemistry of dimethylsulfide in the equatorial Pacific atmosphere, *Geophys. Res. Lett.*, *23*, 741–744, 1996.

Bates, T. S., J. D. Cline, R. H. Gammon, and S. Kelly-Hansen, Regional and seasonal variations in the flux of oceanic dimethylsulfide to the atmosphere, *J. Geophys. Res.*, *92*, 2930–2938, 1987.

Bates, T. S., R. P. Kiene, G. V. Wolfe, P. A. Matrai, F. P. Chavez, K. R. Buck, B. W. Blomquist, and R. L. Cuhel, The cycling of sulfur in surface seawater of the northeast Pacific, *J. Geophys. Res., 99*, 7835–7843, 1994.

Bates, T. S., B. J. Huebert, J. L. Gras, B. Griffiths, and P. A. Durkee, The International Global Atmospheric Chemistry (IGAC) Project's First Aerosol Characterization Experiment (ACE 1): Overview, *J. Geophys. Res.*, this issue.

Berg, O., E. Swietlicki, and R. Krejci, Hygroscopic growth of aerosol particles in the marine boundary layer over the Pacific and Southern Oceans during ACE 1, *J. Geophys. Res.*, this issue.

Berresheim, H., P. H. Wine, and D. D. Davis, Sulfur in the atmosphere, in *Composition, Chemistry, and Climate of the Atmosphere*, vol. 8, edited by H. B. Singh, pp. 251–307, Van Nostrand Reinhold, New York, 1995.

Bigg, E. K., C. Leck, and E. D. Nilsson, Sudden changes in Arctic atmospheric aerosol concentrations during summer and autumn, *Tellus, 48*, 254–271, 1996.

Bond, N. A., and R. G. Fleagle, Prefrontal and postfrontal boundary layer processes over the ocean, *Mon. Weather Rev., 116*, 1257–1273, 1988.

Brechtel, F., S. Kreidenweis, and H. Swan, Air mass characteristics, aerosol particle number concentrations, and number size distributions at Macquarie Island during ACE 1, *J. Geophys. Res.*, this issue.

Chin, M., and D. J. Jacob, Anthropogenic and natural contributions to tropospheric sulfate: A global model analysis, *J. Geophys. Res., 101*, 18,691–18,699, 1996.

Chin, M., D. J. Jacob, G. M. Gardner, N. S. Foreman-Fowler, P. A. Spiro, and D. L. Savoie, A global three-dimensional model of tropospheric sulfate, *J. Geophys. Res., 101*, 18,667–18,690, 1996.

Chuang, C. C., J. E. Penner, K. E. Taylor, A. S. Grossman, and J. J. Walton, An assessment of the radiative effects of anthropogenic sulfate, *J. Geophys. Res., 102*, 3761–3778, 1997.

Clarke, A. D., Atmospheric nuclei in the Pacific midtroposphere: Their nature, concentration, and evolution, *J. Geophys. Res., 98*, 20,633–20,647, 1993.

Clarke, A. D., and J. N. Porter, Pacific marine aerosol, 2, Equatorial gradients, ammonium, and chlorophyll during SAGA3, *J. Geophys. Res., 98*, 16,997–17,101, 1993.

Clarke, A. D., Z. Li, and M. Litchy, Aerosol dynamics in the equatorial Pacific marine boundary layer: Microphysics, diurnal cycles, and entrainment, *Geophys. Res. Lett., 23*, 733–736, 1996.

Clarke, A. D., J. L. Varner, F. Eisele, R. L. Mauldin, D. Tanner, and M. Litchy, Particle production in the remote marine atmosphere: Cloud outflow and subsidence during ACE 1, *J. Geophys. Res.*, this issue.

Cooper, D. J., and E. S. Saltzman, Measurements of atmospheric dimethylsulfide, hydrogen sulfide, and carbon disulfide during GTE/CITE 3, *J. Geophys. Res., 98*, 23,397–23,410, 1993.

Cotton, W. R., G. D. Alexander, R. Hertenstein, R. L. Walko, R. L. McAnelly, and M. Nicholls, Cloud venting—A review and some new global annual estimates, *Earth Sci. Rev., 39*, 169–206, 1995.

Covert, D. S., V. N. Kapustin, P. K. Quinn, and T. S. Bates, New particle formation in the marine boundary layer, *J. Geophys. Res., 97*, 20,581–20,590, 1992.

Covert, D. S., V. N. Kapustin, T. S. Bates, and P. K. Quinn, Physical properties of marine boundary layer aerosol particles of the mid-Pacific in relation to sources and meteorological transport, *J. Geophys. Res., 101*, 6919–6930, 1996a.

Covert, D. S., A. Wiedensohler, P. Aalto, J. Heintzenberg, P. H. McMurry, and C. Leck, Aerosol number size distributions from 3 to 500 nm diameter in the Arctic marine boundary layer during summer and autumn, *Tellus, 48*, 197–212, 1996b.

Covert, D., A. Wiedensohler, and L. M. Russell, Particle charging and transmission efficiencies of aerosol charge neutralizers, *Aerosol Sci. Technol., 27*, 206–214, 1997.

De Bruyn, W. J., T. S. Bates, J. M. Cainey, and E. S. Saltzman, Shipboard measurements of DMS and SO_2 southwest of Tasmania during ACE 1, *J. Geophys. Res.*, this issue.

DeMore, W. B., S. P. Sander, D. M. Golden, R. F. Hampson, M. J. Kurylo, C. J. Howard, A. R. Ravishankara, C. E. Kolb, and M. J. Molina, Chemical kinetics and photochemical data for use in stratospheric modeling, Evaluation No. 10, *JPL Publ., 92-20*, 1992.

Feichter, J., E. Kjellstrom, H. Rodhe, F. Dentener, J. Lelieveld, and G.-J. Roelofs, Simulation of the tropospheric sulfur cycle in a global climate model, *Atmos. Environ., 30*, 1693–1707, 1996.

Galway, J. G., The lifted index as a predictor of latent instability, *Bull. Am. Meteorol. Soc., 37*, 528–529, 1956.

Gong, S. L., L. A. Barrie, and J.-P. Blanchet, Modeling sea-salt aerosols in the atmosphere, 1, Model development, *J. Geophys. Res., 102*, 3805–3818, 1997.

Hainsworth, A., A. L. Dick, and J. L. Gras, Climatic context of ACE 1: A meteorological and chemical overview, *J. Geophys. Res.*, this issue.

Hegg, D. A., L. F. Radke, and P. V. Hobbs, Particle production associated with marine clouds, *J. Geophys. Res., 95*, 13,917–13,926, 1990.

Hegg, D. A., D. S. Covert, and V. N. Kapustin, Modeling a case of particle nucleation in the marine boundary layer, *J. Geophys. Res., 97*, 9851–9857, 1992.

Hoppel, W. A., and G. M. Frick, Submicron aerosol size distributions measured over the tropical and South Pacific, *Atmos. Environ., 24*, 645–659, 1990.

Hoppel, W. A., G. M. Frick, and R. E. Larson, Effect of nonprecipitating clouds on the aerosol size distribution in the marine boundary layer, *Geophys. Res. Lett., 13*, 125–128, 1986.

Hoppel, W. A., J. W. Fitzgerald, G. M. Frick, and R. E. Larson, Aerosol size distributions and optical properties found in the marine boundary layer over the Atlantic Ocean, *J. Geophys. Res., 95*, 3659–3686, 1990.

Hoppel, W. A., G. M. Frick, J. W. Fitzgerald, and R. E. Larson, Marine boundary layer measurements of new particle formation and the effects nonprecipitating clouds have on aerosol size distributions, *J. Geophys. Res., 99*, 14,443–14,459, 1994a.

Hoppel, W. A., G. M. Frick, J. W. Fitzgerald, and B. J. Wattle, A cloud chamber study of the effect that nonprecipitating water clouds have on the aerosol size distribution, *Aerosol Sci. Technol., 20*, 1–30, 1994b.

Kasibhatla, P., W. L. Chameides, and J. St. John, A three-dimensional global model investigation of seasonal variations in the atmospheric burden of anthropogenic sulfate aerosols, *J. Geophys. Res., 102*, 3737–3759, 1997.

Kreidenweis, S., L. McInnes, and F. Brechtel, Observations of aerosol volatility and elemental composition at Macquarie Island during ACE 1, *J. Geophys. Res.*, this issue.

Liss, P. S., and L. Merlivat, Air-sea gas exchange rates: Introduction and synthesis, in *The Role of Air-Sea Exchange in Geochemical Cycling*, edited by P. Buat-Menard, pp. 113–127, D. Reidel, Norwell, Mass., 1986.

Monahan, E. C., D. E. Spiel, and K. L. Davidson, A model of marine aerosol generation via whitecaps and wave distribution, in *Oceanic Whitecaps*, edited by E. C. Monahan and G. Mac Niocaill, pp. 167–174, D. Reidel, Norwell, Mass., 1986.

O'Dowd, C. D., and M. H. Smith, Physico-chemical properties of aerosol over the northeast Atlantic: Evidence for

wind speed related submicron sea-salt aerosol production, *J. Geophys. Res., 98*, 1137–1149, 1993.

O'Dowd, C. D., M. H. Smith, I. E. Consterdine, and J. A. Lowe, Marine aerosol, sea-salt, and the marine sulphur cycle: A short review, *Atmos. Environ., 31*, 73–80, 1997.

Perry, K. D., and P. V. Hobbs, Further evidence for particle nucleation in clear air adjacent to marine cumulus clouds, *J. Geophys. Res., 99*, 22,803–22,818, 1994.

Pham, M., J.-F. Muller, G. P. Brasseur, C. Granier, and G. Megie, A three-dimensional study of the tropospheric sulfur cycle, *J. Geophys. Res., 100*, 26,061–26,092, 1995.

Quinn, P. K., and D. J. Coffman, Local closure during ACE 1: Aerosol mass concentration and scattering and backscattering coefficients, *J. Geophys. Res.*, this issue.

Quinn, P. K., V. N. Kapustin, T. S. Bates, and D. S. Covert, Chemical and optical properties of marine boundary layer aerosol particles of the mid-Pacific in relation to sources and meteorological transport, *J. Geophys. Res., 101*, 6931–6952, 1996.

Quinn, P. K., D. J. Coffman, V. N. Kapustin, T. S. Bates, and D. S. Covert, Aerosol optical properties in the marine boundary layer during ACE 1 and the underlying chemical and physical aerosol properties, *J. Geophys. Res.*, this issue.

Raes, F., Entrainment of free-tropospheric aerosol as a regulating mechanism for cloud condensation nuclei in the remote marine boundary layer, *J. Geophys. Res., 100*, 2893–2903, 1995.

Raes, F., and R. Van Dingenen, Simulations of condensation nuclei and cloud condensation nuclei from biogenic SO_2 in the remote marine boundary layer, *J. Geophys. Res., 97*, 12,901–12,912, 1992.

Russell, L. M., S. N. Pandis, and J. H. Seinfeld, Aerosol production and growth in the marine boundary layer, *J. Geophys. Res., 99*, 20,989–21,003, 1994.

Saltzman, E. S., S. A. Yvon, and P. A. Matrai, Low level detection of atmospheric sulfur dioxide measurements using HPLC/Fluorescence detection, *J. Atmos. Chem., 17*, 73–90, 1993.

Shaw, G. E., Production of condensation nuclei in clean air by nucleation of H_2SO_4, *Atmos. Environ., 23*, 2841–2846, 1989.

Sievering, H., J. Boatman, E. Gorman, Y. Kim, L. Anderson, G. Ennis, M. Luria, and S. Pandis, Removal of sulphur from the marine boundary layer by ozone oxidation in sea-salt aerosol, *Nature, 360*, 571–573, 1992.

Sievering, H., E. Gorman, T. Ley, A. Pszenny, M. Springer-Young, J. Boatman, Y. Kim, C. Nagamoto, and D. Wellman, Ozone oxidation of sulfur in sea-salt aerosol particles during the Azores Marine Aerosol and Gas Exchange experiment, *J. Geophys. Res., 100*, 23,075–23,081, 1995.

Spivakovsky, C. M., R. Yevich, J. A. Logan, S. C. Wofsy, M. B. McElroy, and M. J. Prather, Tropospheric OH in a three-dimensional chemical tracer model: An assessment based on observations of CH_3CCl_3, *J. Geophys. Res., 95*, 18,441–18,471, 1990.

Taylor, K. E., and J.E. Penner, Response of the climate system to atmospheric aerosols and greenhouse gases, *Nature*, 369, 734-737, 1994.

Thornton, D.C., A. R. Bandy, B. W. Blomquist, D. D. Davis, and R. W. Talbot, Sulfur dioxide as a source of condensation nuclei in the upper troposphere of the Pacific Ocean, *J. Geophys. Res., 101*, 1883–1890, 1996.

Wanninkhof, R. H., Relationship between wind speed and gas exchange over the ocean, *J. Geophys. Res., 97*, 7373–7382, 1992.

Weber, R. J., and P. H. McMurry, Fine particle size distributions at the Mauna Loa Observatory, Hawaii, *J. Geophys. Res., 101*, 14,767–14,775, 1996.

Weber, R. J., P. H. McMurry, F. L. Eisele, and D. J. Tanner, Measurement of expected nucleation precursor species and 3–500 nm diameter particles at Mauna Loa Observatory, Hawaii, *J. Atmos. Sci., 52*, 2242–2257, 1995.

Weber, R. J., J. J. Marti, P. H. McMurry, F. L. Eisele, D. J. Tanner, and A. Jefferson, Measured atmospheric new particle formation rates: Implications for nucleation mechanisms, *Chem. Eng. Commun., 151*, 53–64, 1996.

Weber, R. J., J. J. Marti, P. H. McMurry, F. L. Eisele, D. J. Tanner, and A. Jefferson, Measurements of new particle formation and ultrafine particle growth rates at a clean continental site, *J. Geophys. Res., 102*, 4375–4385, 1997.

Weber, R. J., P. H. McMurry, L. Mauldin, D. J. Tanner, F. L. Eisele, F. J. Brechtel, S. M. Kreidenweis, G. L. Kok, R. D. Schillawski, and D. Baumgardner, A study of new particle formation and growth involving biogenic trace gas species measured during ACE 1, *J. Geophys. Res.*, this issue.

Whittlestone, S., and W. Zahorowski, Baseline radon detectors for shipboard use: Development and deployment in ACE 1, *J. Geophys. Res.*, this issue.

Wiedensohler, A., D. S. Covert, E. Swietlicki, P. Aalto, J. Heintzenberg, and C. Leck, Occurrence of an ultrafine particle mode less than 20 nm in diameter in the marine boundary layer during Arctic summer and autumn, *Tellus, 48*, 213–222, 1996.

Wiedensohler, A., et al., Intercomparison study of size dependent counting efficiency of 26 condensation particle counters, *Aerosol Sci. Technol., 27*, 224–242, 1997.

Yvon, S. A., E. S. Saltzman, D. J. Cooper, T. S. Bates, and A. M. Thompson, Atmospheric dimethylsulfide cycling at a tropical South Pacific station (12°S, 135°W): A comparison of field and model results, *J. Geophys. Res., 101*, 6899–6910, 1996.

T. S. Bates and P. K. Quinn, Pacific Marine Environmental Laboratory, NOAA, 7600 Sand Point Way NE, Seattle, WA 98115. (e-mail: bates@pmel.noaa.gov; quinn@pmel.noaa.gov)

D. J. Coffman, D. S. Covert, and V. N. Kapustin, Joint Institute for the Study of the Atmosphere and Ocean (JISAO), University of Washington, Seattle, WA 98195. (e-mail: derek@pmel.noaa.gov; covert@u.washington.edu; kapustin@soest.hawaii.edu)

W. J. De Bruyn and E. S. Saltzman, RSMAS, University of Miami, Miami, FL 33124. (e-mail: debruyn@rsmas.miami.edu; esaltzman@rsmas.miami.edu)

P. A. Durkee, Department of Meteorology, Naval Postgraduate School, Monterey, CA 93943. (e-mail: durkee@nps.navy.mil)

C. Mari, Laboratoire d'Aerologie (UPS/CNRS 5560), Observatoire Midi Pyrenees, 14, avenue Edouard Belin, 31400 Toulouse, France. (e-mail: marc@aero.obs-mp.fr)

(Received June 2, 1997; revised December 18, 1997; accepted December 18, 1997.)